ACS APPLIED NANO MATERIALS

www.acsanm.org Letter

van der Waals Heterostructures Based on Nanolayered Paramagnetic Tm(II) Compounds and Boron Nitride for Investigating Spin Frustration

William N. G. Moore, Timothy J. McSorley, Alexandre Vincent, Joseph W. Ziller, Luis A. Jauregui,* and William J. Evans*

Cite This: *ACS Appl. Nano Mater.* 2023, 6, 6461−6466 Read Online

ACCESS | Metrics & More | Article Recommendations | Supporting Information

ABSTRACT: The utility of molecular precursors to create thin-film components for constructing van der Waals heterostructures was explored by studying the layered Tm(II) compound $[(THF)Cs(\mu\text{-}\eta^5\text{:}\eta^5\text{-}Cp')_3Tm^{II}]_n$ (Cp′ = $C_5H_4SiMe_3$). This compound, synthesized by the reduction of Cp'_3Tm^{III} with metallic cesium, crystallizes as layers of hexagonal nets composed of Tm(II) ions and Cs(I) ions at alternating vertices, bridged by Cp′ ligands. Full characterization of the compound, including SQUID magnetometry, was consistent with $4f^{13}$ Tm(II). Though the triangular orientation of $S = 1/2$ Tm(II) ions in the layered structure indicated a potential environment for spin frustration, the SQUID data suggest these metal centers lack enough interaction to enforce such behavior. Successful exfoliation of the air- and moisture-sensitive single crystals was achieved in a glovebox at low temperatures to yield thin films. These could be stacked under hexagonal boron nitride to create an air-stable van der Waals heterostructure, which allowed analysis by AFM to determine a thickness of approximately 50 layers for the covered Tm-containing structure.

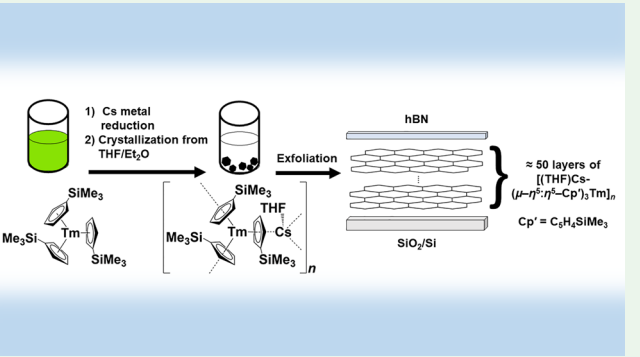

KEYWORDS: *van der Waals, exfoliation, heterostructure, thin film, rare-earth metal*

INTRODUCTION

Thin films have garnered significant interest recently, as they have been shown to exhibit unusual emergent properties.[1−7] The range of synthetic methods used to generate these materials includes chemical vapor deposition (CVD),[8] liquid exfoliation,[5,9] chemical growth,[10] spin-coating techniques (SCT),[11] layer-by-layer (LbL) assembly deposition,[12] and mechanical exfoliation of available layered solid-state materials.[13,14] Exfoliation is advantageous in that the bulk properties of a material can be elucidated prior to the generation of thin films.

The materials most suitable for exfoliation to thin films are classified as van der Waals (vdW) materials, which are characterized as having layered solid-state structures in which there are strong bonds in two dimensions but only weak interlayer interactions at distances greater than or equal to 3 Å in the third dimension.[15] Interest in this class of materials was sparked with the initial exfoliation of graphene,[13] and subsequent studies of atomically thin layers have facilitated growing interest in this area.[16] New exfoliation methods have been developed, including micromechanical exfoliation with Scotch or Nitto low-residue tape,[17] sonication,[18] and commercial blending.[19]

Solid-state compounds with layered structures like graphite, boron nitride, and transition-metal dichalcogenides (TMDs) are well-studied vdW materials, but the variety available is limited.[15] New layered materials can be manufactured by stacking films of these precursor materials on top of each other, but the number of starting materials is not large.[20] The construction of thin-film heterostructures from molecular precursors synthesized in solution is a less-explored area that has the potential to dramatically increase the array of possible compositions for thin films.[9] In addition, solution-phase chemistry could be used to rationally design the specific components of the thin films. This has some precedent for these known vdW materials[9] and would be beneficial to extend to new systems such as those that contain rare-earth metal ions. Rare-earth metal-containing thin films synthesized via

Received: February 12, 2023
Accepted: March 29, 2023
Published: April 6, 2023

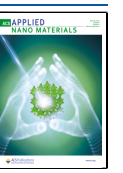

https://doi.org/10.1021/acsanm.3c00662
ACS Appl. Nano Mater. 2023, 6, 6461−6466

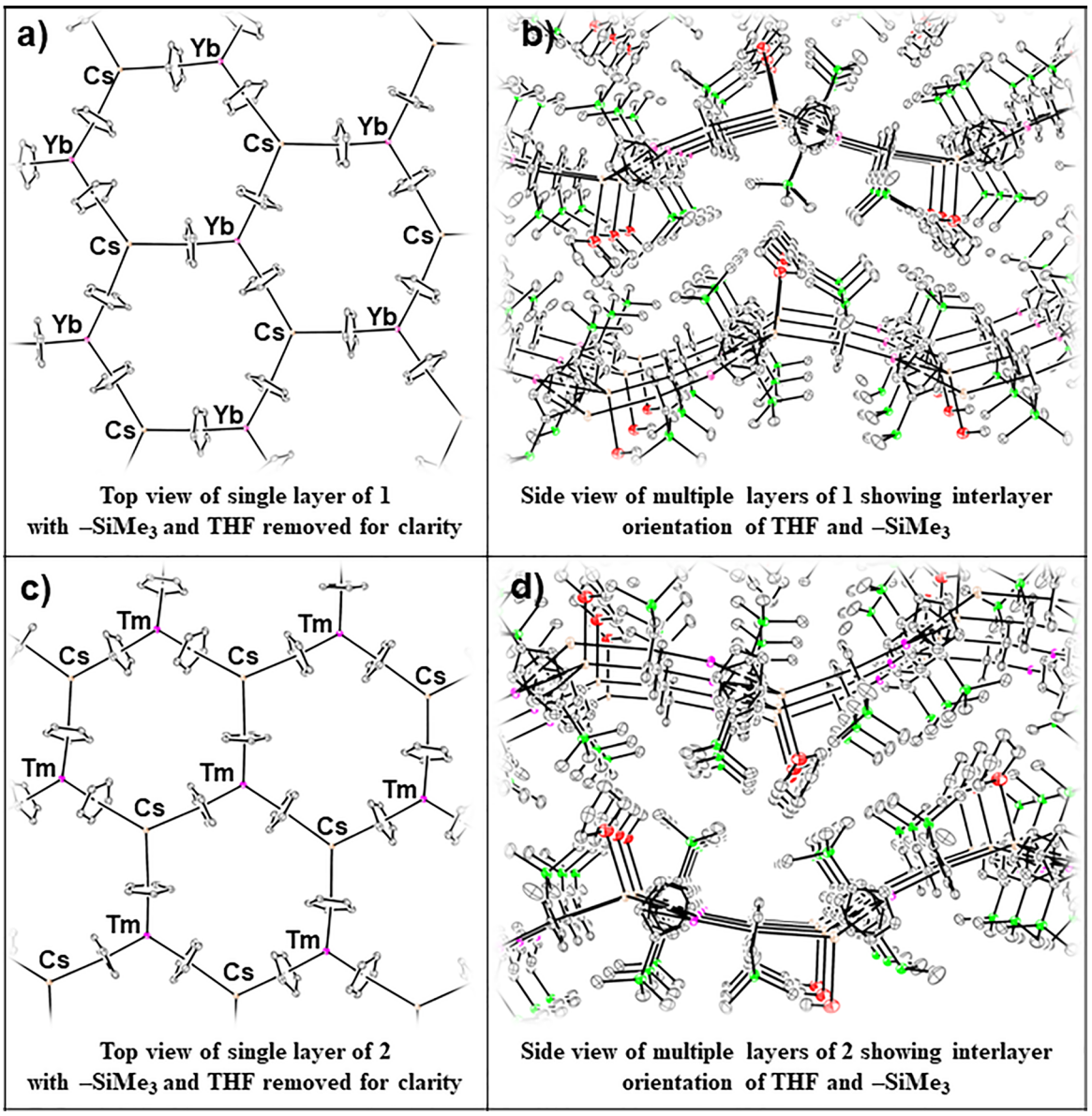

Figure 1. ORTEP of extended structures of both $[(THF)Cs(\mu\text{-}\eta^5\text{:}\eta^5\text{-}Cp')_3Yb^{II}]_n$ (**1**) and $[(THF)Cs(\mu\text{-}\eta^5\text{:}\eta^5\text{-}Cp')_3Tm^{II}]_n$ (**2**). All displacement ellipsoids are drawn at the 50% probability level (magenta, Tm; pink, Yb; tan, Cs; green, Si; red, O).

other methods are garnering interest as molecular sensors,[21] luminescent materials,[22] and spin liquid candidates.[23]

Recently, an organometallic rare-earth compound, $[(THF)Cs(\mu\text{-}\eta^5\text{:}\eta^5\text{-}Cp')_3Yb^{II}]_n$ (**1**; Cp′ = $C_5H_4SiMe_3$), was synthesized and found to have a layered structure (see Figure 1) that could potentially be exfoliated to form thin films.[24] Compound **1** is one of several recent structures that crystallize with layers of hexagonal networks comprised of three M(II) ions (M = Ba, Yb, and U) and three Cs(I) ions connected by bridging Cp′ ligands.[25,26] The trimethylsilyl groups of the Cp′ ligand and the methylene groups of the bound THF molecules extend outward perpendicular to the layer plane but do not form covalent bonds with other layers. The interlayer distance of approximately 1.8 Å between these functional groups is on the shorter side for a vdW material, but this crystal system seemed promising for exfoliation studies. Moreover, it is notable that the layered structure appears robust in the face of changing M(II) ions.[25] In fact, the THF solvation level can vary as well, tuning the planarity of the layered structure.[25]

Substituting diamagnetic Yb(II) with a paramagnetic analogue was of interest because the hexagonal network incorporates these ions in a triangular orientation that offers the potential for spin frustration at low temperatures. In order to explore the exfoliation of this type of structure with an S = 1/2 paramagnetic compound, rather than diamagnetic **1**, the $4f^{13}$ Tm(II) analogue $[(THF)Cs(\mu\text{-}\eta^5\text{:}\eta^5\text{-}Cp')_3Tm^{II}]_n$ (**2**), was synthesized. Reported here are the synthesis and X-ray crystal structure of **2**, its characterization by SQUID magnetometry as an $^2F_{7/2}$ Tm(II) compound, and its successful exfoliation to make a heterostructure with hexagonal boron nitride. Synthesizing otherwise inaccessible crystal lattices (heavy elements/rare earths/more complex geometries) that can be incorporated into a nanodevice/heterostructure with other two-dimensional layered materials can create new opportunities in materials science, engineering, and physics.

https://doi.org/10.1021/acsanm.3c00662
ACS Appl. Nano Mater. 2023, 6, 6461−6466

RESULTS AND DISCUSSION

Synthesis and X-ray Crystal Structure. $[(THF)Cs(\mu\text{-}\eta^5{:}\eta^5\text{-}Cp')_3Tm^{II}]_n$ (**2**) was synthesized by reduction of Cp'_3Tm^{III} with a cesium smear in THF at −35 °C (eq 1),

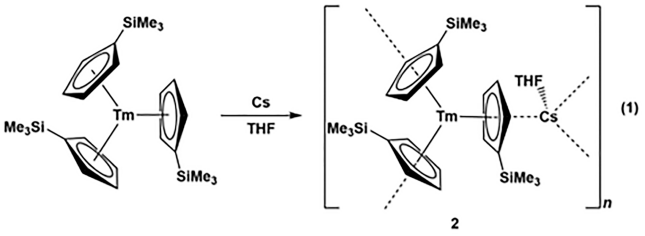

resulting in a color change from lime green to dark green/black. Crystallization by slow vapor diffusion of Et_2O into a concentrated THF solution of **2** at −35 °C yielded dark green/black hexagonal blocks approximately 0.276 × 0.288 × 0.628 mm in size. Single-crystal X-ray diffraction studies revealed that compound **2** (Figure 1) is isomorphous with compound **1**.

The bond distances and angles in **2** (see Table S2) are similar to those in **1**, which is consistent with the similar radial sizes of Tm(II) and Yb(II). There are also metrical similarities between **2** and the closely related nonlayered complex $[K(crypt)][Cp'_3Tm^{II}]$ (**3**).[27] For example, the 2.501 Å Tm−Cp'_{cnt} (Cp'_{cnt} = centroid of Cp′) distance in **2** is similar to the Tm−Cp'_{cnt} distances of 2.509 and 2.502 Å observed in **1** and **3**, respectively. The layers in **2** are corrugated, as shown by the 20.17° dihedral angle between adjacent mean planes of six metal ions. Furthermore, the root-mean-square deviation (RMSD, ω_{hex}) of the six metal ions from the mean plane of their positions is ω_{hex} = 0.669 Å, versus ω_{hex} = 0 for a completely planar structure. These data are similar to those for the Yb(II) analogue **1**: ω_{hex} = 0.671 and dihedral angle 20.26°.[24] This observed consistency between **1** and **2** demonstrates that the corrugated nature of the individual layers is not impacted by changing the M(II) center from Yb(II) to Tm(II).

Spectroscopic and Magnetic Properties. The solution-phase characterization of **2** via multinuclear NMR and UV−visible absorption spectroscopy was conducted in THF, since **2** is insoluble in solvents such as diethyl ether, toluene, and hexanes, and it is reactive toward other solvents such as acetonitrile and dimethylformamide. The UV−visible absorption spectrum of **2** features bands centered at 430 nm (ε = 600 $M^{-1}cm^{-1}$) and 645 nm (ε = 300 $M^{-1}cm^{-1}$), as well as a shoulder at 340 nm (ε = 700 $M^{-1}cm^{-1}$) (Figure S1). The molar absorptivities are consistent with f → d Laporte-allowed transitions typical for Tm(II) complexes.[27] The spectrum of **2** is quite similar to the spectrum of **3**, which displays absorbances at 416, 550, and 634 nm.[27] The Raman spectrum of **2** is silent from 0 to 2500 cm^{-1} using 405, 532, and 785 nm lasers (Figures S2−S4).

The variable-temperature magnetic susceptibility of **2** (Figure 2) was measured under applied fields of 0.1, 0.5, and 1 T to establish the ground-state electron configuration of the thulium ions and to evaluate the exchange interactions present. The room-temperature $\chi_M T$ product was found to be approximately 3.4 K•emu/mol under each of the three applied fields. Upon fitting these data sets in PHI,[28] the results were found to be consistent with a single unique ion in a $^2F_{7/2}$ electronic ground state possessing temperature-independent paramagnetism (TIP) along with weak intermolecular exchange on the order of 10^{-2} cm^{-1}. These results are consistent with a $4f^{13}$ thulium electron configuration, which is typical for other Tm(II)-containing complexes.[29] The vanishingly weak magnetic exchange observed was in line with expectations, since the Tm(II) ions are spatially isolated from their nearest neighbors by two closed-shell cyclopentadienyl ligands and a bridging Cs(I) ion.

$$\hat{H} = g_J \mu_B \hat{J}_{Tm} \cdot \vec{B} \tag{2}$$

Despite the paramagnetic nature of **2**, ^1H and ^{133}Cs NMR spectra were observable (Figures S5 and S6). Resonances in the ^1H NMR spectrum of **2** are broadened with a full-width at half-maximum (fwhm) of 230 Hz that is consistent with its paramagnetism. A single ^{133}Cs resonance is observed for **2** at −218.62 ppm, and it is nearly identical with that of the previously characterized Yb(II) analogue (δ = −218.18 ppm).[25] This suggests that the cesium cations have similar chemical environments in solution. No signal was observed in the X-band CW EPR spectrum of **2** taken in perpendicular mode at 77 K, which is consistent with the strong spin−orbit coupling associated with the anisotropic $4f^{13}$ electron configuration that induces relatively fast electron relaxation.

Exfoliation. In order to obtain thin layers of **2**, a sample of **2** was mechanically exfoliated using blue Nitto low-residue

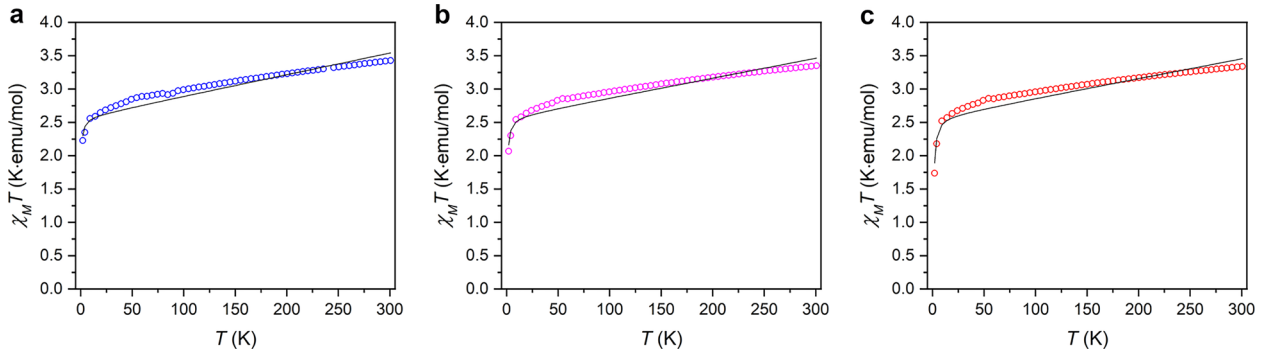

Figure 2. Variable-temperature magnetic susceptibility of **2** from 2 to 300 K. Fitted curves are shown as black traces. Fits were obtained in a $|J,M_J\rangle$ basis using the Hamiltonian given in eq 2. Open circles correspond to experimental data. Applied fields and fit parameters with their parenthesized uncertainties are reported. (a) H = 0.1 T, zJ = −0.024(4) cm^{-1}, TIP = 0.00323(4) K•emu/mol. (b) H = 0.5 T, zJ = −0.0312(4) cm^{-1}, TIP = 0.00297(4) K•emu/mol. (c) H = 1 T, zJ = −0.043(6) cm^{-1}, TIP = 0.00295(4) K•emu/mol. The intermolecular interaction (zJ) between spins was modeled using the mean-field approximation as implemented in PHI.[28]

https://doi.org/10.1021/acsanm.3c00662
ACS Appl. Nano Mater. 2023, 6, 6461−6466

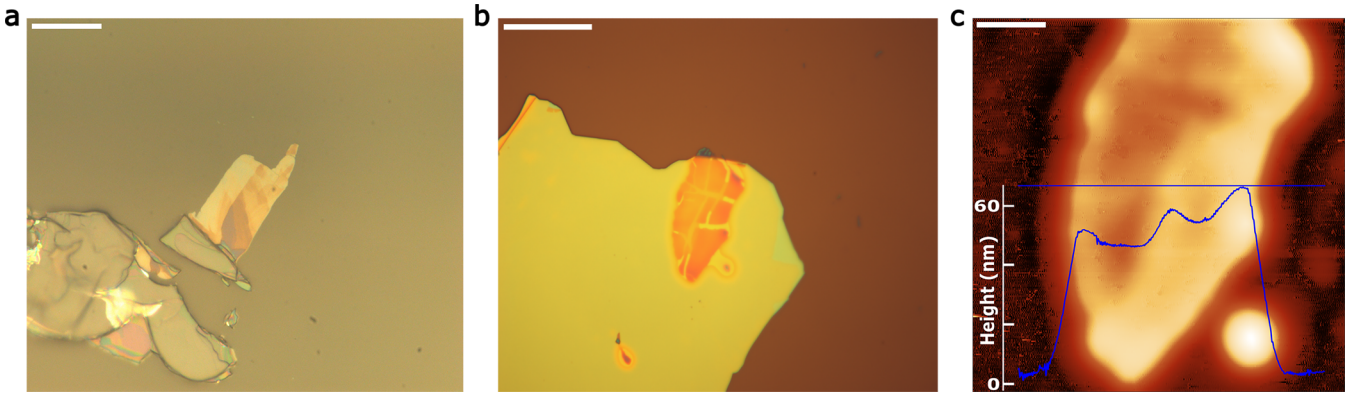

Figure 3. Characterization of thin layers of **2**. (a) Optical image of a sample of exfoliated thin flakes of **2** on PDMS (sample a). The scale bar is 20 μm. (b) Optical image of sample b encapsulated by hBN. The scale bar is 25 μm. (c) AFM image of sample b. The inset shows the step height along the blue trace. The scale bar is 5 μm.

tape under an argon atmosphere inside a glovebox. The tape was then adhered to a small slab of polydimethylsiloxane (PDMS) that was precooled to −35 °C. Lowering the temperature of the PDMS closer to its glass transition temperature has been shown to improve its adhesion properties.[30] After removing the tape from the cold PDMS, thin layers of **2** were deposited on the surface of the PDMS. These layers were then transferred onto a SiO_2/Si substrate for further studies. After imaging several thin layers, films containing steps of different thicknesses were observed, demonstrating the layered nature of **2** (Figure 3a). In order to protect the samples from exposure to water or oxygen, the exfoliated flakes were covered with hexagonal boron nitride (hBN) as shown in Figure 3b. The Raman spectrum of the sample collected with a 532 nm laser displayed no absorbances between 100 and 2500 cm^{-1} (Figure S7), consistent with the spectrum of the bulk crystals.

Atomic Force Microscopy (AFM). Topographical characterization of the sample in Figure 3b was performed using an atomic force microscope. This allowed an estimate of the number of layers within the hBN encapsulated flake. From the optical microscope images, differences in contrast indicated that the sample was composed of regions of varying thicknesses. In Figure 3c, two plateaus of relatively constant thickness can be observed, one at 50 nm and another at 58 nm. With a single-layer thickness of approximately 10 Å, this suggests that the sample in Figure 3b is approximately 50 layers thick.

CONCLUSION

The synthesis of a layered paramagnetic Tm(II) compound, $[(THF)Cs(\mu\text{-}\eta^5{:}\eta^5\text{-}Cp')_3Tm^{II}]_n$ (**2**) from the reduction of Cp'_3Tm^{III} with cesium in THF provided an opportunity to determine if heterostructures could be constructed from molecular species generated in solution. Compound **2** was fully characterized by single-crystal X-ray crystallography, UV−visible and NMR spectroscopy, and magnetic measurements that show **2** is a $4f^{13}\ ^2F_{7/2}$ Tm(II) compound. Air- and moisture-sensitive single crystals of **2** were exfoliated to thin films (approximately 50 layers in thickness) and successfully covered with hexagonal boron nitride to make a heterostructure. This demonstrates the viability of using molecularly designed compounds of this type for the construction of heterostructures. Given the robust nature of complex **2** and the synthetic capability to tailor the lanthanide starting material, it is of interest to incorporate more magnetically interesting lanthanides into this system in the future. In fact, the incorporation of dysprosium or terbium may lead to antiferromagnetic behavior that would be applicable in various systems such as spintronics, memory/storage devices, and THz devices.[31]

EXPERIMENTAL DETAILS

All manipulations and syntheses described below were conducted with the rigorous exclusion of air and water using standard Schlenk line and glovebox techniques under an argon atmosphere. Solvents were sparged with UHP argon and dried by passage through columns containing Q-5 and molecular sieves prior to use. Deuterated THF was dried for 1 week over NaK alloy, degassed by three freeze−pump−thaw cycles, and vacuum-transferred before use. ^1H and ^{133}Cs NMR spectra were recorded on a GN500 MHz spectrometer. The ^1H NMR spectrum was collected at 298 K and referenced internally to residual protio-solvent resonances. The ^{133}Cs spectrum was collected at 298 K and referenced to $CsNO_3$ following the recommended scale based on ratios of absolute frequencies.[32] UV−visible absorbance spectra were collected on an Agilent Cary 60 UV−vis spectrometer. Infrared spectra were collected on an Agilent Cary 630 spectrometer equipped with a diamond ATR attachment. EPR spectra were collected using the X-band frequency (9.3−9.8 GHz) on a Bruker EMX spectrometer equipped with an ER4119HS-W1 microwave bridge. Cesium (>99.5%, Aldrich) was used as received in the ampule sealed under argon. Cp'_3Tm was synthesized via the literature procedure.[27]

All magnetic measurements were carried out on a Quantum Design MPMS-XL SQUID magnetometer. Under an atmosphere of argon, crystals of **2** were mechanically ground into a fine powder, 12.0 mg of which was loaded into a quartz tube (inner diameter 5 mm, outer diameter 7 mm). The powder was covered with a solid layer of eicosane (50.3 mg) and flame-sealed under vacuum. The eicosane was subsequently melted at 45 °C in order to restrain the sample (prevent crystallite torquing) and to improve thermal conductivity between the sample and the environment. Diamagnetic corrections were calculated using Pascal's constants[33] and were applied to all reported magnetic susceptibility values unless otherwise noted.

$[(THF)Cs(\mu\text{-}\eta^5{:}\eta^5\text{-}Cp')_3Tm]_n$ (2). Under an argon atmosphere, a vial with Cp'_3Tm (45 mg, 0.08 mmol) dissolved in THF (1.5 mL) and a vial with a cesium smear were precooled to −35 °C. The light green THF solution of Cp'_3Tm was transferred by pipet into the vial containing the cesium smear, and the heterogeneous mixture was stirred for 5 min at room temperature, over which time the color changed to dark black/green. The solvent was removed in vacuo, and the remaining solids were washed with cold hexanes. Extraction with THF and removal of the solvent under reduced pressure yielded a black microcrystalline material (42 mg, 69%). Black crystals of

https://doi.org/10.1021/acsanm.3c00662
ACS Appl. Nano Mater. 2023, 6, 6461−6466

$[(THF)Cs(\mu\text{-}\eta^5{:}\eta^5\text{-}Cp')_3Tm]_n$ that were suitable for study by single-crystal X-ray crystallography were grown by slow vapor diffusion of Et_2O into a concentrated THF solution at −35 °C. ^1H NMR (500 MHz, THF-d_8): δ 19.81 (s, 6H), δ 5.51 (s, 6H), δ − 0.05 (s, 27H). ^{133}Cs NMR (65 MHz, THF-d_8): δ − 218.62 (s). IR ν, cm^{-1}: 3073w, 2947w, 2893w, 1438w, 1400w, 1353w, 1306w, 1242m, 1176m, 1035m, 903m, 824s, 742s, 680m. UV−visible λ_{max}, nm (ε, M^{-1} cm^{-1}): 340 (700), 430 (600), 645 (300). Anal. Calcd for $[(THF)Cs(\mu\text{-}\eta^5{:}\eta^5\text{-}Cp')_3Tm]$, $[C_{28}H_{47}CsOSi_3Tm]$: C, 42.80; H, 6.03. Found: C, 35.65; H, 5.698. Incomplete combustion was observed as has been found in the past with complexes of this type,[34] but the observed CH ratio was $C_{28}H_{53}$.

Heterostructure Formation. h-BN crystals exfoliated via thermal release tape were transferred onto a stamp of PDMS by applying the tape to the surface of the stamp and peeling it off. A large uniform flake of hBN was optically located on the PDMS and subsequently transferred to a SiO_2/Si chip with recently exfoliated Tm(II) material. This was achieved by aligning both hBN and Tm(II) flakes, using a robotic transfer stage with 12 degrees of freedom inside an argon-filled glovebox. Once the flakes were aligned, the stamp was slowly lowered until the BN was in contact with the Tm(II) flakes. The system was heated to 80 °C, and the stamp was slowly lifted until out of contact. The hBN flake was left behind on top of the Tm(II) flake, encapsulating it.

■ ASSOCIATED CONTENT

Data Availability Statement

CCDC 2248022 contains the supplementary crystallographic data for this paper. These data can be obtained free of charge via www.ccdc.cam.ac.uk/data_request/cif, or by emailing data_request@ccdc.cam.ac.uk, or by contacting The Cambridge Crystallographic Data Centre, 12 Union Road, Cambridge CB2 1EZ, UK; fax: + 44 1223 336033.

Supporting Information

The Supporting Information is available free of charge at https://pubs.acs.org/doi/10.1021/acsanm.3c00662.

UV−visible absorption, NMR, and IR spectra as well as crystallographic details for **2** (PDF)

■ AUTHOR INFORMATION

Corresponding Authors

Luis A. Jauregui − *Department of Physics, University of California, Irvine, California 92697, United States*; Email: lajaure1@uci.edu

William J. Evans − *Department of Chemistry, University of California, Irvine, California 92697, United States*; orcid.org/0000-0002-0651-418X; Email: wevans@uci.edu

Authors

William N. G. Moore − *Department of Chemistry, University of California, Irvine, California 92697, United States*; orcid.org/0000-0001-5074-9341

Timothy J. McSorley − *Department of Physics, University of California, Irvine, California 92697, United States*; orcid.org/0000-0001-8367-1595

Alexandre Vincent − *Department of Chemistry, University of California, Berkeley, California 94720, United States*; orcid.org/0000-0002-9134-0435

Joseph W. Ziller − *Department of Chemistry, University of California, Irvine, California 92697, United States*; orcid.org/0000-0001-7404-950X

Complete contact information is available at: https://pubs.acs.org/10.1021/acsanm.3c00662

Notes

The authors declare no competing financial interest.

■ ACKNOWLEDGMENTS

We thank the U.S. National Science Foundation for support of this research under CHE-2154255 (to W.J.E.), NSF-CAREER DMR 2146567 (to L.A.J.), and CHE-2102603 (to A.V. and Professor Jeffrey R. Long at the University of California, Berkeley). Furthermore, we thank the Eddleman Quantum Institute for developing the collaboration that led to this study and for an Eddleman Quantum Institute Graduate Fellowship (to T.J.M.). This work was partially supported by the NSF Materials Research Science and Engineering Center program through the UC Irvine Center for Complex and Active Materials (DMR-2011967).

■ REFERENCES

(1) Novoselov, K. S.; Jiang, D.; Schedin, F.; Booth, T. J.; Khotkevich, V. V.; Morozov, S. V.; Geim, A. K. Two-Dimensional Atomic Crystals. *Proc. Natl. Acad. Sci. U. S. A.* **2005**, *102*, 10451−10453.

(2) Novoselov, K. S.; Fal'Ko, V. I.; Colombo, L.; Gellert, P. R.; Schwab, M. G.; Kim, K. A Roadmap for Graphene. *Nature* **2012**, *490*, 192−200.

(3) Lee, C.; Wei, X.; Kysar, J. W.; Hone, J. Measurement of the Elastic Properties and Intrinsic Strength of Monolayer Graphene. *Science* **2008**, *321*, 385−388.

(4) Peng, Y.; Li, Y.; Ban, Y.; Jin, H.; Jiao, W.; Liu, X.; Yang, W. Metal-Organic Framework Nanosheets as Building Blocks for Molecular Sieving Membranes. *Science* **2014**, *346*, 1356−1359.

(5) Nicolosi, V.; Chhowalla, M.; Kanatzidis, M. G.; Strano, M. S.; Coleman, J. N. Liquid Exfoliation of Layered Materials. *Science* **2013**, *340*, 72−75.

(6) Bradshaw, D.; Garai, A.; Huo, J. Metal−Organic Framework Growth at Functional Interfaces: Thin Films and Composites for Diverse Applications. *Chem. Soc. Rev.* **2012**, *41*, 2344−2381.

(7) Ajayan, P.; Kim, P.; Banerjee, K. Two-Dimensional van Der Waals Materials. *Phys. Today* **2016**, *69*, 38−44.

(8) Tang, L.; Tan, J.; Nong, H.; Liu, B.; Cheng, H. M. Chemical Vapor Deposition Growth of Two-Dimensional Compound Materials: Controllability, Material Quality, and Growth Mechanism. *Accounts Mater. Res.* **2021**, *2*, 36−47.

(9) Han, J. H.; Kwak, M.; Kim, Y.; Cheon, J. Recent Advances in the Solution-Based Preparation of Two- Dimensional Layered Transition Metal Chalcogenide Nanostructures. *Chem. Rev.* **2018**, *118*, 6151−6188.

(10) Bonilla, M.; Kolekar, S.; Ma, Y.; Diaz, H. C.; Kalappattil, V.; Das, R.; Eggers, T.; Gutierrez, H. R.; Phan, M. H.; Batzill, M. Strong Roomerature Ferromagnetism in VSe_2 Monolayers on van Der Waals Substrates. *Nat. Nanotechnol.* **2018**, *13*, 289−293.

(11) Polai, B.; Satpathy, B. K.; Jena, B. K.; Nayak, S. K. An Overview of Coating Processes on Metal Substrates Based on Graphene-Related Materials for Multifarious Applications. *Ind. Eng. Chem. Res.* **2022**, *61*, 13763−13786.

(12) Santos, J. C. C.; Pramudya, Y.; Krstić, M.; Chen, D. H.; Neumeier, B. L.; Feldmann, C.; Wenzel, W.; Redel, E. Halogenated Terephthalic Acid "Antenna Effects" in Lanthanide-SURMOF Thin Films. *ACS Appl. Mater. Interfaces* **2020**, *12*, 52166−52174.

(13) Novoselov, K. S.; Geim, A. K.; Morozov, S. V.; Jiang, D.; Zhang, Y.; Dubonos, S. V.; Grigorieva, I. V.; Firsov, A. A. Electric Field in Atomically Thin Carbon Films. *Science* **2004**, *306*, 666−669.

(14) Wang, Y.; Ziebel, M. E.; Sun, L.; Gish, J. T.; Pearson, T. J.; Lu, X. Z.; Thorarinsdottir, A. E.; Hersam, M. C.; Long, J. R.; Freedman, D. E.; Rondinelli, J. M.; Puggioni, D.; Harris, T. D. Strong Magnetocrystalline Anisotropy Arising from Metal-Ligand Covalency in a Metal-Organic Candidate for 2D Magnetic Order. *Chem. Mater.* **2021**, *33*, 8712−8721.

(15) Duong, D. L.; Yun, S. J.; Lee, Y. H. Van Der Waals Layered Materials: Opportunities and Challenges. *ACS Nano* **2017**, *11*, 11803−11830.
(16) Bhimanapati, G. R.; Lin, Z.; Meunier, V.; Jung, Y.; Cha, J.; Das, S.; Xiao, D.; Son, Y.; Strano, M. S.; Cooper, V. R.; Liang, L.; Louie, S. G.; Ringe, E.; Zhou, W.; Kim, S. S.; Naik, R. R.; Sumpter, B. G.; Terrones, H.; Xia, F.; Wang, Y.; Zhu, J.; Akinwande, D.; Alem, N.; Schuller, J. A.; Schaak, R. E.; Terrones, M.; Robinson, J. A. Recent Advances in Two-Dimensional Materials beyond Graphene. *ACS Nano* **2015**, *9*, 11509−11539.
(17) Chahal, S.; Ranjan, P.; Motlag, M.; Yamijala, S. S. R. K. C.; Late, D. J.; Sadki, E. H. S.; Cheng, G. J.; Kumar, P. Borophene via Micromechanical Exfoliation. *Adv. Mater.* **2021**, *33*, 2102039.
(18) Gosch, J.; Synnatschke, K.; Stock, N.; Backes, C. Comparative Study of Sonication-Assisted Liquid Phase Exfoliation of Six Layered Coordination Polymers. *Chem. Commun.* **2022**, *59*, 55−58.
(19) Ng, K. L.; Maciejewska, B. M.; Qin, L.; Johnston, C.; Barrio, J.; Titirici, M.-M.; Tzanakis, I.; Eskin, D. G.; Porfyrakis, K.; Mi, J.; Grobert, N. Direct Evidence of Exfoliation Efficiency and Graphene Dispersibility of Green Solvents towards Sustainable Graphene Production. *ACS Sustainable Chem. Eng.* **2022**, *11*, 58−66.
(20) Meng, J.; Wang, D.; Cheng, L.; Gao, M.; Zhang, X. Recent Progress in Synthesis, Properties, and Applications of Hexagonal Boron Nitride-Based Heterostructures. *Nanotechnology* **2019**, *30*, 074003.
(21) Qu, X. L.; Yan, B. Ln(III)-Functionalized Metal-Organic Frameworks Hybrid System: Luminescence Properties and Sensor for Trans, Trans-Muconic Acid as a Biomarker of Benzene. *Inorg. Chem.* **2018**, *57*, 7815−7824.
(22) Chen, P.; Xu, X.; Li, D.; Li, Z.; Wang, H.; Pi, L.; Zhou, X.; Zhai, T. 2D Van Der Waals Rare Earth Material Based Ratiometric Luminescence Thermography Integrated on Micro−Nano Devices Vertically. *Adv. Opt. Mater.* **2022**, *10*, 2102102.
(23) Chamorro, J. R.; McQueen, T. M.; Tran, T. T. Chemistry of Quantum Spin Liquids. *Chem. Rev.* **2021**, *121*, 2898−2934.
(24) Huh, D. N.; Ziller, J. W.; Evans, W. J. Crystal Structure of the $[(THF)Cs(\mu\text{-}\eta^5{:}\eta^5\text{-}Cp')_3Yb]_n$ Oligomer. *Acta Crystallogr. Sect. E Crystallogr. Commun.* **2020**, *76*, 1131−1135.
(25) Huh, D. N.; Ciccone, S. R.; Moore, W. N. G.; Ziller, J. W.; Evans, W. J. Synthesis of Ba(II) Analogs of Ln(II)-in-(2.2.2-Cryptand) and Layered Hexagonal Net Ln(II) Complexes, $[(THF)Cs(\mu\text{-}\eta^5{:}\eta^5\text{-}C_5H_4SiMe_3)_3Ln^{II}]_n$. *Polyhedron* **2021**, *210*, 115493.
(26) Huh, D. N.; Ziller, J. W.; Evans, W. J. Chelate-Free Synthesis of the U(II) Complex, $[(C_5H_3(SiMe_3)_2)_3U]^{1-}$, Using Li and Cs Reductants and Comparative Studies of La(II) and Ce(II) Analogs. *Inorg. Chem.* **2018**, *57*, 11809−11814.
(27) Fieser, M. E.; Macdonald, M. R.; Krull, B. T.; Bates, J. E.; Ziller, J. W.; Furche, F.; Evans, W. J. Structural, Spectroscopic, and Theoretical Comparison of Traditional vs Recently Discovered Ln^{2+} Ions in the $[K(2.2.2\text{-Cryptand})][(C_5H_4SiMe_3)_3Ln]$ Complexes: The Variable Nature of Dy^{2+} and Nd^{2+}. *J. Am. Chem. Soc.* **2015**, *137*, 369−382.
(28) Chilton, N. F.; Anderson, R. P.; Turner, L. D.; Soncini, A.; Murray, K. S. PHI: A Powerful New Program for the Analysis of Anisotropic Monomeric and Exchange-Coupled Polynuclear d- and f-Block Complexes. *J. Comput. Chem.* **2013**, *34*, 1164−1175.
(29) Moutet, J.; Schleinitz, J.; La Droitte, L.; Tricoire, M.; Pointillart, F.; Gendron, F.; Simler, T.; Clavaguéra, C.; Le Guennic, B.; Cador, O.; Nocton, G. Bis-Cyclooctatetraenyl Thulium(II): Highly Reducing Lanthanide Sandwich Single-Molecule Magnets. *Angew. Chemie - Int. Ed.* **2021**, *60*, 6042−6046.
(30) Clarson, S. J.; Dodgson, K.; Semlyen, J. A. Studies of cyclic and linear poly(dimethylsiloxanes): 19. glass transition temperatures and crystallization behaviour,. *Polymer* **1985**, *26* (6), 930−934.
(31) Rahman, S.; Torres, J. F.; Khan, A. R.; Lu, Y. Recent Developments in van der Waals Antiferromagnetic 2D Materials: Synthesis, Characterization, and Device Implementation. *ACS Nano* **2021**, *15*, 17175−17213.
(32) Harris, R. K.; Becker, E. D.; Cabral De Menezes, S. M.; Granger, P.; Hoffman, R. E.; Zilm, K. W. Further conventions for NMR shielding and chemical shifts: (IUPAC recommendations 2008). *Pure Appl. Chem.* **2008**, *80*, 59−84.
(33) Bain, G. A.; Berry, J. F. Diamagnetic Corrections and Pascal's Constants. *J. Chem. Educ.* **2008**, *85*, 532−536.
(34) Ortu, F.; Packer, D.; Liu, J.; Burton, M.; Formanuik, A.; Mills, D. P. Synthesis and structural characterization of lanthanum and cerium substituted cyclopentadienyl borohydride complexes. *J. Organomet. Chem.* **2018**, *857*, 45−51.

https://doi.org/10.1021/acsanm.3c00662
ACS Appl. Nano Mater. 2023, 6, 6461−6466